RSC Advances

ROYAL SOCIETY
OF CHEMISTRY

www.rsc.org/advances

Atomic Structures and Electronic Properties of Ta-Doped 2*H*-NbSe$_2$

Hongping Li,[a,*] Shuai Liu,[a] Lin Chen,[a] Jun Wu,[a] Peng Zhang,[a] Hua Tang,[a]

Changsheng Li,[a] Xiaojuan Liu,[b] Zhongchang Wang,[c] Jian Meng,[b,*]

[a]*Institute for Advanced Materials, School of Materials Science and Engineering, Jiangsu University, Zhenjiang, 212013, P. R. China*
[b]*State Key Laboratory of Rare Earth Resources Utilization, Changchun Institute of Applied Chemistry, Chinese Academy of Sciences, Changchun, 130022, P. R. China*

[c]*Advanced Institute for Materials Research, Tohoku University, 2-1-1 Katahira, Aoba-ku, Sendai 980-8577, Japan*

Abstract: Chemical doping represents one of the most effective ways to precisely modulate material performances for target technological applications. Here, we report, by first-principles calculations, the impact of Ta doping on the crystal structures and electronic properties of the technologically relevant 2*H*-NbSe$_2$. We have considered a total of three Ta-doping models and demonstrated that the most thermodynamically stable one is that the Ta atoms are located at the center of the octahedra comprising of Se atoms. Further structural analysis uncovers that the Ta-doped 2*H*-NbSe$_2$ maintains the original structure, yet shows an enhanced electronic property, which may benefit the realization of superconducting nature of 2*H*-NbSe$_2$. We also find a hybridization of the Ta 5d and Se 4p orbitals and a marked degree of charge transfer between Ta and Se, forming a strong covalency for the Ta-Se bonds. Moreover, we also find that the tensile strain can remarkably enhance charge transferr in this system. Our calculations suggest that the transition-metal doping shall serve as a useful way to tailor electronic

structures of 2*H*-NbSe$_2$ so as to improve its electronic properties.

Introduction

Layered transition metal dichalcogenides (LTMDs), a class of graphene-like materials, have aroused extensive interest recently due to their quasi-two-dimensional and highly anisotropic structures, making them versatile as candidates for the thin and flexible devices as well as for various other applications such as lubrication, catalysts, transistors, electrochemical photocells and lithium-ion batteries.[1–6] Structurally, the LTMDs have a chemical formula of MX$_2$ (M: transition metal, X: chalcogen), which comprises one M layer sandwiched in between two X layers, forming edge-sharing MX$_6$ octahedra with a strong covalent bonding in plane. However, the out-of-plane X-M-X layers are coupled only by weak van der Waals (vdW) interactions, offering a practical feasibility for exfoliating the LTMDs to ultrathin layers and for intercalating impurities into them so as to tailor their electronic and physical properties.

2*H*-NbSe$_2$, a representative of LTMDs, is well known for its charge density wave (CDW) state below 39 K and highest superconducting transition ever reported among the LTMDs family (7.4 K).[7–9] It is even quite special due to its CDW instability and coexistence or competition with superconductivity that arise from the instability of the Fermi surface and electron-phonon interaction. To date, a huge number of chemical modifications and physical measurements have been carried out on 2*H*-NbSe$_2$, aimed at altering its Fermi surface topology in order to manipulate its properties. One typical manner to tune remarkably electronic behavior is *via* chemical doping of 2*H*-NbSe$_2$,

including V,[10,11] Cr,[12] Mn,[13] Fe,[13–15] Co,[15] Cu[14–16] and Ge[17]. For example, the effect of

magnetic field and atomic impurities on the CDW transition has been reported for the

$2H$-NbSe$_2$ revealing an intriguing connection between the CDW and superconducting

states.[13] It is also reported that the Cu intercalation can not only change the electronic

structures of $2H$-NbSe$_2$, but also affect its Fermi surface topology and corresponding

nesting condition.[16] A $2a_0 \times 2a_0$ hexagonal superstructure is observed in the Cu$_{1/4}$NbSe$_2$

at surface, which is attributed to the change in the local density of states caused by the

charge transfer between the intercalated and surface atoms.[15] A significant amount of

electrons are introduced to $2H$-NbSe$_2$ in the Fe- and Cu-intercalated LTMD Fe$_x$NbSe$_2$

and Cu$_x$NbSe$_2$, resulting in the band downshifting and/or folding.[14] In addition, a

bump-like resistivity anomaly is observed at ~100 K and magnetization is found to

increase rapidly at low temperature in Nb$_{1-x}$V$_x$Se$_2$.[10] Combining optical spectroscopy

observations with first-principles calculations, Wang *et al*. detected a band broadening

effect across a ferromagnetic transition in Cr$_{1/3}$NbSe$_2$.[12]

Albeit that the macroscopic functionality of $2H$-NbSe$_2$ can be markedly modified

by intercalating foreign metallic atoms into the weakly bonded layers, it remains hard

to extract atomistic information on how the impurities can impact the electronic and

physical properties of $2H$-NbSe$_2$, which is a timely and relevant issue for the device

applications. Here, we investigate systematically, by the first-principles calculations,

the effects of Ta-doping on atomic structures and electronic properties of $2H$-NbSe$_2$.

The Ta is chosen purposely because it is a transition metal and locates in the same

subgroup with Nb. In addition, Ta and Nb have a very close atomic and ionic size

(0.82 and 0.68 Å, respectively), thereby suggesting that Ta substitution in $2H$-NbSe$_2$ might give rise to a minimum lattice distortion and hence a stable doped model. We find that the Ta doping is chemically preferred and can improve electronic properties by showing an increased density of states (DOS) around Fermi level (E_F).

Computational details

Calculations of energies and electronic structures were performed using the plane-wave pseudopotential method implemented in the Cambridge Sequential Total Energy Package (CASTEP) Code.[18] The Broyden-Fletcher-Goldfrab-Shanno (BFGS) method was used to carry out the geometrical optimization. The generalized gradient approximation (GGA) within the Perdew-Burke-Ernzerhof scheme was employed to describe the exchange-correlation potential.[19,20] The plane-wave cut-off energy was adopted to be 400 eV and the Monkhorst-Pack[21] grid parameter for k-point was set to 6×6×3 in the Brillouin zone. The valence electron configuration for the Nb, Ta and Se was $4s^24p^64d^45s^1$, $5d^36s^2$ and $4s^24p^4$, respectively. The phonon properties were calculated using the linear-response method[22,23]. The self-consistency was achieved once the total energy was converged to less than $1.0×10^{-5}$ eV and the magnitude of force on each atom fell below 0.03 eV/Å.

Results and Discussion

Crystal Structure and Thermodynamic Stability

$2H$-NbSe$_2$ crystallizes in the hexagonal phase with a space group P6$_3$/mmc,[24] in

which Nb and Se atoms are linked covalently in the triple layers forming edge-sharing

$NbSe_6$ octahedra (Fig. 1(a)). The Se-Nb-Se layers stack along c-axis and are coupled

by the weak vdW interactions. The 2×2×1 supercells are adopted to simulate both the

pristine and Ta-doped systems.[25] The calculated optimum lattice constants (Table 1)

are a = 6.909 Å and c = 12.806 Å,[26] slightly larger than the experimental values (a =

6.889 Å and c = 12.544 Å)[24]. These data are, however, consistent with the previous

calculations,[11,27,28] validating the application of our calculation method. To investigate

how the Ta doping at different sites affects crystal structures and electronic properties

of $2H$-$NbSe_2$, we considered three possible models: *i*) substituted model in which a

Nb atom is replaced by a Ta atom (Fig. 1(b)) (named S-doping), *ii*) intercalated model

in which a Ta atom is intercalated in the empty octahedral position between the $NbSe_2$

layers (Fig. 1(c)) (named I-doping), and *iii*) embedded model in which a Ta atom is

embedded into the in-plane Nb-Se hexahedral voids (Fig. 1(d)) (named E-doping). We

first performed a geometrical optimization of the models and ruled out the possibility

of the E-doping model because it cannot converge into a stable state at all and the

Nb-Se hexahedron undergoes a severely distortion.

The formation enthalpy (ΔE_H), which is defined as the difference in total energy

of the sum of products minus the sum of the reactants, can be used to analyze the

relative stability of the doped systems, as can be expressed as follows:

$$\Delta E_{H\ (S\text{-doping})} = E_{(S\text{-doping})} - E_{(pure)} - \mu_{Ta} + \mu_{Nb}$$

$$\Delta E_{H\ (I\text{-doping})} = E_{(I\text{-doping})} - E_{(pure)} - \mu_{Ta}$$

where $E_{(pure)}$ is total energy of the host $2H$-$NbSe_2$ supercell, $E_{(S\text{-doping})}$ and $E_{(I\text{-doping})}$ are

total energies of the S-doping and I-doping supercells, and μ_{Ta} and μ_{Nb} are chemical potentials of Ta and Nb atom calculated from their corresponding bulk. The ΔE_H is calculated to be +0.253 eV for the S-doping and -1.597 eV for the I-doping, which implies that I-doping is thermodynamically stable at ambient condition. The S-doping sample can merely be prepared with the assistance of external stimuli such as the high temperature and high pressure. Hence, we will mainly show the I-doping results in the following discussion.

Structurally, geometrical optimization reveals that the I-doping model still holds the P6$_3$/mmc space group with a = 6.926 Å and c = 13.008 Å, notwithstanding a little lattice distortion. An extension of its unit cell along the c-axis (~ 0.202 Å) is observed after Ta intercalation, which is accompanied by a volume expansion (529.402 Å^3 for the pristine 2H-NbSe$_2$ whereas 540.528 Å^3 in the I-doping case). The in-plane lattice constant is, however, extended slightly by ~0.015 Å. Interestingly, the six Ta-Se bonds have the same length (2.589 Å), which means that the intercalated Ta is located at the center of the octahedron comprising of Se atoms, as what was seen in Ge-intercalated Ge$_x$NbSe$_2$.[17] Nevertheless, it is shorter than those calculated from the effective ionic radii of Ta and Se (0.68 Å and 1.98 Å), suggesting a strong covalent hybridization interactions between the Ta and Se. Furthermore, the nearest NbSe$_6$ octahedra around the Ta are somewhat distorted, which is characterized by the variation of the Nb-Se bond length from 2.587 to 2.634 Å (2.598 Å in pristine 2H-NbSe$_2$).

Electronic Structures

To shed light on the impact of the Ta-doping on electronic property of $2H$-NbSe$_2$, we first conducted the band structure and DOS analyses of pristine $2H$-NbSe$_2$. Fig. 2(a) shows band structure of the pristine $2H$-NbSe$_2$, revealing a metallic nature with several bands across the E_F, consistent with the experimental results.[7] Such a metallic character is also reflected in the DOS plot (Fig. 3(a)), showing a high density around E_F, in agreement with the bands with a weak dispersion around E_F (Fig. 2(a)). It is noteworthy that the E_F sits precisely at a peak of the states, implying that $2H$-NbSe$_2$ may be superconducting.[7] Further analysis of partial DOS (PDOS) demonstrates that Nb 4d and Se 4p orbitals contribute dominantly to the remarkable DOS around E_F. Importantly, the PDOSs of Nb and Se are rather broad in energy ranging from -5.7 eV to 3.2 eV, and located almost in the same energy area, indicative of strong covalent hybridization interactions between the Nb and Se atoms.

To understand the effect of Ta doping on magnetic interaction in $2H$-NbSe$_2$, we take into account both non-spin-polarized and spin-polarized configurations. We first find that the spin-polarized configuration is more favorable than non-spin-polarized one by saving 0.405 eV, indicating that an ordered magnetic array can be induced by Ta doping in this system, as seen in the ferromagnetic transition in Nb$_{1-x}$V$_x$Se$_2$ and Cr$_{1/3}$NbSe$_2$.[10,12] The calculated magnetic moment for Ta atom is 0.99 μ_B, while all the other atoms maintain nonmagnetic states. Fig. 2(b) and 2(c) shows band structure of the Ta-doped $2H$-NbSe$_2$, from which one can see an asymmetry in the spin-up and spin-down bands, indicating a magnetic property. It is noteworthy that the number of electronic bands around E_F is increased significantly, especially in the spin-up channel,

which consequently strengthens its metallic character. Furthermore, the band gap in conduction band is disappeared after doping due to the Ta 5d states, which benefits the electronic property of $2H$-NbSe$_2$.

Figure 3(b) shows DOS of Ta-doped $2H$-NbSe$_2$, where one can see that the E_F is obviously upshifted as compared with that in the pristine case, a characteristic of the n-type doping nature. The occupied electronic concentration is increased dramatically by introducing impurity states, which accounts for the upshift in E_F. This phenomenon has been confirmed by the angle-resolved photoemission observation in intercalated LTMDs Fe$_x$NbSe$_2$ and Cu$_x$NbSe$_2$, in which a significant amount of electrons are introduced into $2H$-NbSe$_2$, resulting in the downshifting of the original bands in pure $2H$-NbSe$_2$.[14] In particular, the Se atoms gain more electrons than Nb atoms because their PDOS is transferred to deeper energy region, indicating a strong covalent hybridization interaction between Se and Ta. Moreover, the spin-up channel of Ta is partly filled, while its spin-down channel is almost empty, demonstrating that Ta is responsible for realizing its magnetic nature because the PDOS of Nb or Se atoms is symmetric. Importantly, Ta 5d, Nb 4d and Se 4p orbitals hybridize nearly in the whole energy range from -6.8 eV to 3.2 eV. Interestingly, the Ta 5d orbitals are even wider than the Nb 4d, implying that the Ta-Se bonds have a larger level of covalency than the Nb-Se. This is also verified by the bond population analysis showing that bond population of the Ta-Se bonds (0.40) is larger than that of the Nb-Se bonds (0.31).

We further present in Fig. 4 charge-density contour plot along the (110) plane for both the pristine and Ta-doped $2H$-NbSe$_2$. Evidently, the charge density distribution is

connected between the Ta and Se, giving rise to covalency for the Ta-Se bonds in the Ta-doped $2H$-NbSe$_2$. Further, the Ta is found to be almost ionized with a significant amount of electrons transferred to its neighboring Se. To gain more insights into the effect of Ta doping, we show in Fig. 5 electronic structure of the nearest neighboring (NN) and the second nearest neighboring (SN) Se atoms around Ta. The PDOS results reveal that there is a pronounced influence of Ta on the NN Se due to downshifting of PDOS to lower energy, while its impact on other Se atoms is subtle, indicating that the electrons introduced by Ta doping are mainly transferred to its neighboring Se atoms. To further quantitatively study charge transfer, we calculate the Mulliken populations. The Mulliken charge of the NN Se is calculated to be +0.23, while that of the SN Se is calculated to be +0.20, indicating that the Ta releases more electrons into the NN Se atoms. We therefore believe that the doping of transition metals should be regarded as a useful way to modulate the electronic structures so as to improve conducting or even realize superconducting properties of $2H$-NbSe$_2$.

Mechanical and Vibrating Properties

We also investigated the impact of external strain on the electronic behaviors of the Ta-doped $2H$-NbSe$_2$, as shown in Fig. 6. Both the compressive and tensile biaxial strains are applied to Ta-doped $2H$-NbSe$_2$ with the maximum amplitude of 6%. The biaxial strain is defined as $\varepsilon = \Delta a/a$, where a is the unstrained lattice parameter, and Δa is its corresponding variation. One can see that DOS in the case of compressive strain is pushed to high energy area, while that in the case of tensile strain is pushed to the

low energy area. The degree of such DOS shift is enhanced with increasing tensile strain, similar to what was observed in the $NbSe_2$ monolayer,[27] which may enhance charge transfer and hence electronic property. These results indicate that mechanical strain enables to alter electronic properties of Ta-doped 2*H*-$NbSe_2$.

Moreover, we also conducted the phonon calculations to investigate the vibrating property of the Ta-doped 2*H*-$NbSe_2$. Fig. 7 shows the calculated phonon dispersion curves along the high-symmetry directions in Brillouin zone and the corresponding total and atom-projected phonon DOS. From Fig. 7(a), soft modes (only two curves) around the high-symmetry G point are observed in the full phonon dispersion, which suggests that the external stimuli could lead to the atomic vibrations and consequently realize phase transition, as reported in $Nb_{1-x}V_xSe_2$,[10]. Further, one can notice that the phonon spectra almost have no gaps, which can mainly be attributed to the small mass difference between Nb and Se atoms. All phonon modes are somewhat degenerate at the high-symmetry F and Q points. In addition, the frequencies of some optical modes are close to those of some acoustic modes, indicating that it is easy to transfer energy between these modes. According to non-harmonic effects, these low-frequency optical modes will strongly scatter acoustic modes, which carry the heat flow and may result in low lattice thermal conductivity.[29] The vacancy of the vibration band gaps can also be verified by the calculated total phonon DOS (Fig. 7(b)). It is noteworthy that the presence of localized states indicates that the lattice vibration at the corresponding frequency is similar with atomic state.[30] In addition, the highest phonon frequencies are mainly attributed to the Nb atom vibrations, while the lowest phonon frequencies

10

are mainly from Ta atom vibrations (Fig. 7(c)), indicating that the atoms (M_{Ta}=180.95 Da) with a larger mass dominate acoustic phonons, and those (M_{Nb}=92.91 Da) with a less mass dominate optical phonons.

Conclusions

We have conducted a first-principles calculation of the atomistic structures and electronic properties of pristine and Ta-doped 2*H*-NbSe$_2$, aimed at investigating how the doping can impact electronic properties of 2*H*-NbSe$_2$. A total of three Ta-doping models have been constructed and our calculated formation enthalpy reveals that the most favorable structure is the one that the Ta atoms are located at the center of the octahedra comprising of Se atoms. The 2*H*-NbSe$_2$ structure is maintained after doping albeit that the c-axis is expanded. We have also found that the electronic property is enhanced after doping, which may benefit the realization of superconducting nature of 2*H*-NbSe$_2$. The intercalated Ta is almost ionized, and most of the introduced electrons are transferred to the nearest neighboring Se, which should account for the strong covalency of the Ta–Se bonds. Moreover, the electronic structure is also found to be altered by tensile strain. Such a remarkable modification of electronic structure allows us a straightforward method to identify the effective doping in layered 2*H*-NbSe$_2$, and also provides an additional avenue to modulate material performance in LTMDs.

Acknowledgments

*Corresponding authors

E-mails: hpli@mail.ujs.edu.cn (H.L.); jmeng@ciac.ac.cn (J.M.)

TEL: +86-511-88783268

Notes and references

1. L. Rapoport, N. Fleischer and R. Tenne, *J. Mater. Chem.*, 2005, **15**, 1782.

2. R. Tenne, *Nat. Nanotechnol.*, 2006, **1**, 103.

3. Y. F. Yu, S. Y. Huang, Y. P. Li, S. N. Steinmann, W. T. Yang and L. Y. Cao, *Nano Lett.*, 2014, **14**, 553.

4. B. Radisavljevic, A. Radenovic, J. Brivio, V. Giacometti and A. Kis, *Nat. Nanotechnol.*, 2011, **6**, 147.

5. Q. H. Wang, K. Kalantar-Zadeh, A. Kis, J. N. Coleman and M. S. Strano, *Nat. Nanotechnol.*, 2012, **7**, 699.

6. H. J. Chen, Y. Xie, H. L. Cui, W. Zhao, X. L. Zhu, Y. M. Wang, X. J. Lü and F. Q. Huang, *Chem. Commun.*, 2014, **50**, 4475.

7. E. Boaknin, M. A. Tanatar, J. Paglione, D. Hawthorn, F. Ronning, R. W. Hill, M. Sutherland, L. Taillefer, J. Sonier, S. M. Hayden and J. W. Brill, *Phys. Rev. Lett.,* 2003, **90**, 117003.

8. T. Yokoya, T. Kiss, A. Chainani, S. Shin, M. Nohara and H. Takagi, *Science*, 2001, **294**, 2518.

9. C. D. Malliakas and M. G. Kanatzidis, *J. Am. Chem. Soc.,* 2013, **135,** 1719.

10. I. Naik, G. C. Tiwari, C. S. Yadav and A. K. Rastogi, *Indian J. Phys.*, 2013, **87**, 1075.

11. L. Chen, C. S. Li, H. Tang, H. P. Li, X. J. Liu and J. Meng, *RSC Adv.*, 2014, **4**, 9573.

12. W. Z. Hu, G. T. Wang, R. W. Hu, C. Petrovic, E. Morosan, R. J. Cava, Z. Fang and N. L. Wang, *Phys. Rev. B.*, 2008, **78**, 085120.

13. R. C. Morris, *Phys. Rev. Lett.,* 1975, **34**, 1164.

14. Y. Koh, S. Cho, J. Lee, L. X. Yang, Y. Zhang, C. He, F. Chen, D. L. Feng, M. Arita and K. Shimada, *Jpn. J. Appl. Phys.*, 2013, **52**, 10MC15.

15. A. Prodan, V. Marinković, M. Rojšek, N. Jug, H. J. P. van Midden, F. W. Boswell, J. C. Bennett and H. Böhm, Surf. Sci., 2001, **476**, 71.

16. Y. Y. Koh, Y. K. Kim, W. S. Jung, G. R. Han, S. R. Park, C. S. Leem, Chul Kim, D. J. Song, W. S. Kyung, H.Y. Choi, L. X. Yang, C. He, F. Chen, D. L. Feng and C.Kim, *J. Phys. Chem. Solids*, 2011, **72**, 565.

17. M. Kars, A. Gómez-Herrero, A. Rebbah and L.C. Otero-Diáz, Mater. Res. Bull., 2009, **44**, 1601.

18. M. D. Segall, P. J. D. Lindan, M. J. Probert, C. J. Pickard, P. J. Hasnip, S. J. Clark and M. C. Payne, *J. Phys. Condens. Matter*, 2002, **14**, 2717.

19. H. J. Monkhorst and J. D. Pack, *Phys. Rev. B*, 1976, **13**, 5188.

20. J. D. Pack and H. J. Monkhorst, *Phys. Rev. B*, 1977, **16**, 1748.

21. J. P. Perdew, K. Burke and M. Ernzerhof, *Phys. Rev. Lett.*, 1996, **77**, 3865.

22. X. Gonze and C. Lee, *Phys. Rev. B*, 1997, **55**, 10355.

23. S. Baroni, S. D. Gironcoli, A. D. Corso and P. Giannozzi, *Rev. Mod. Phys.*, 2001, **73**, 515.

24. M. Marezio, P. D. Dernier, A. Menth and G. W. Hull Jr., *J. Solid State Chem.*, 1972, **4**, 425.

25. We also conducted electronic structure calculations using the $3\times3\times1$ and $4\times4\times1$ supercells to investigate the size effect, and found that electronic structures do not undergo fundamental change by the supercell size.

26. H. P. Li, L. Chen, K. Zhang, J. Q. Liang, H. Tang, C. S. Li, X. J. Liu, J. Meng and Z. C. Wang, *J. Appl. Phys.*, 2014, **116**, 103709.

27. Y. G. Zhou, Z. G. Wang, P. Yang, X. T. Zu, L. Yang, X. Sun and F. Gao, *ACS Nano*, 2012, **6**, 9727.

28. A. Kumar and P. K. Ahluwalia, *J. Alloys Compd.*, 2013, **550**, 283.

29. Y. L. Li, W. L. Fan, H. G. Sun, X. F. Cheng, P. Li and X. Zhao, *J. Appl. Phys*, 2009, **106**, 033704.

30. A. Togo, L. Chaput, I. Tanaka and G. Hug, *Phys. Rev. B*, 2010, **81**, 174301.

Table 1 The optimized structural parameters of the adopted 2×2×1 supercell, selected bond lengths, and calculated formation enthalpy (ΔE_H) for the pristine and I-doping 2*H*-NbSe$_2$. The experimental structural parameters are given for comparison.

	a, b, c (Å)	α, β, γ(°)	V(Å^3)	Nb-Se (Å)	Ta-Se(Å)	ΔE_H(eV)
[a]NbSe$_2$	a=6.889 b=6.889 c=12.544	α=90.000 β=90.000 γ=120.000	517.456	2.623 × 6	---	---
[b]NbSe$_2$	a=6.909 b=6.909 c=12.806	α=90.000 β=90.000 γ=120.007	529.402	2.598 × 6	---	---
I-doping	a=6.926 b=6.926 c=13.008	α=89.981 β=90.019 γ=119.984	540.528	2.587 × 3 2.634 × 3	2.589× 6	-1.597

[a]The experimental results of pristine 2*H*-NbSe$_2$ in ref. 24.

[b]The calculated results of pristine 2*H*-NbSe$_2$ in ref. 26.

Fig. 1 Side views of the 2×2×1 supercells for the pristine and Ta-doped 2*H*-NbSe$_2$. (a) pristine 2*H*-NbSe$_2$, (b) S-doping with a Nb atom replaced by a Ta, (c) I-doping with a Ta atom intercalated into octahedral position of the van der Waals gap between NbSe$_2$ layers, and (d) E-doping with a Ta atom embedded into the in-plane Nb-Se hexahedral void.

Fig. 2 Band structure diagrams for pristine and spin-polarized Ta-doped 2*H*-NbSe$_2$ along the major symmetric directions: (a) pristine 2*H*-NbSe$_2$, (b) the spin-up and (c) spin-down bands for Ta-doped 2*H*-NbSe$_2$. The dashed and horizontal lines define the Fermi level.

Fig. 3 Total DOS and PDOS for (a) pristine and (b) Ta-doped 2*H*-NbSe$_2$. The Fermi level is aligned to zero and indicated by a vertical dashed line.

Fig. 4 Contour plots of charge densities for (a) pristine and (b) Ta-doped 2*H*-NbSe$_2$ viewed along the (110) plane.

Fig. 5 PDOSs for the nearest neighboring (I-doping NN) and the secondly nearest neighboring (I-doping SN) Se atoms around the Ta in the Ta-doped 2*H*-NbSe$_2$. The corresponding spin-poralized plot for Se in the pure 2*H*-NbSe$_2$ (pure) is also given for comparison. The Fermi level is aligned to zero and indicated by a vertical dashed line.

16

Fig. 6 Total DOS of Ta-doped $2H$-NbSe$_2$ under different biaxial strain. The Fermi level is aligned to zero and indicated by a vertical dashed line.

Fig. 7 Phonon dispersion curves (a) along the high symmetry directions and (b) total and (c) partial phonon DOS for Ta-doped $2H$-NbSe$_2$.
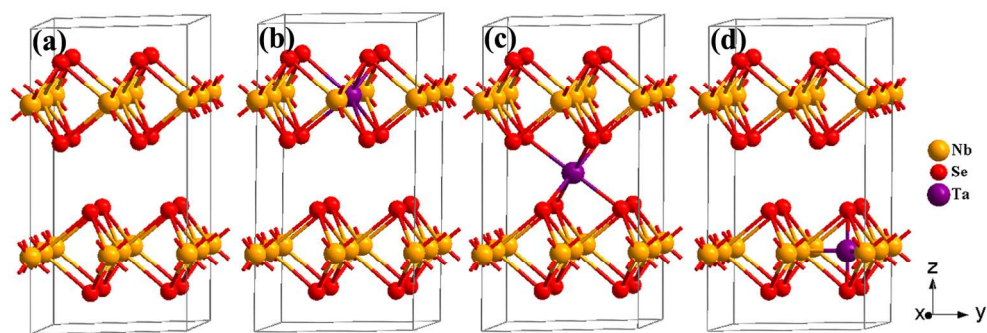
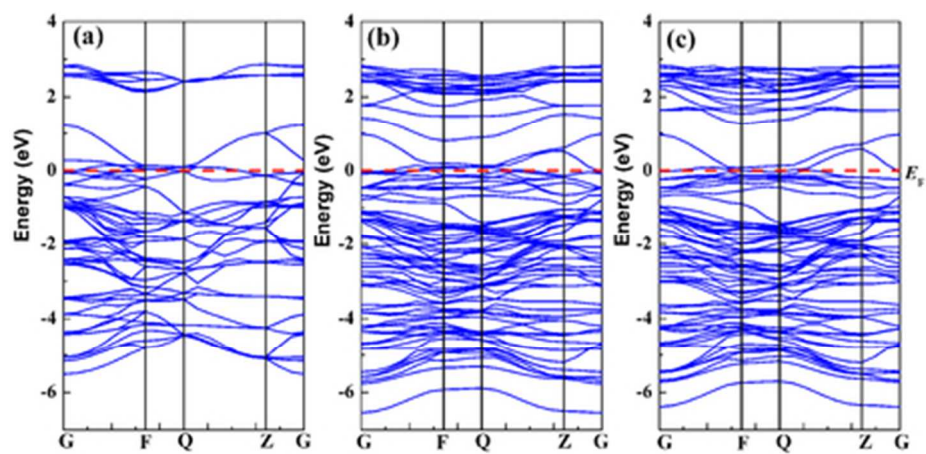Fig.1
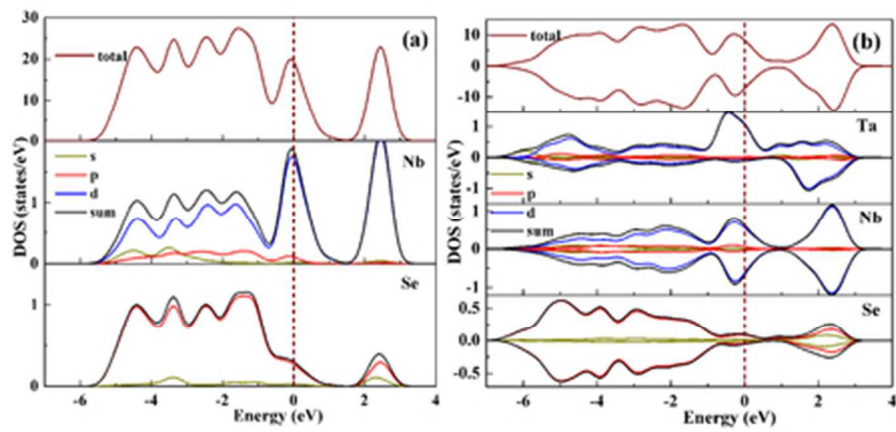160x56mm (300 x 300 DPI)
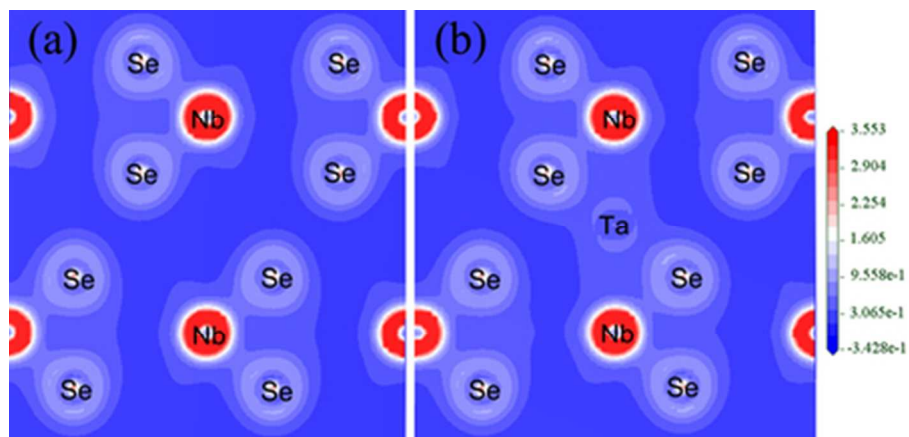
Fig.2
38x18mm (300 x 300 DPI)

Fig.3
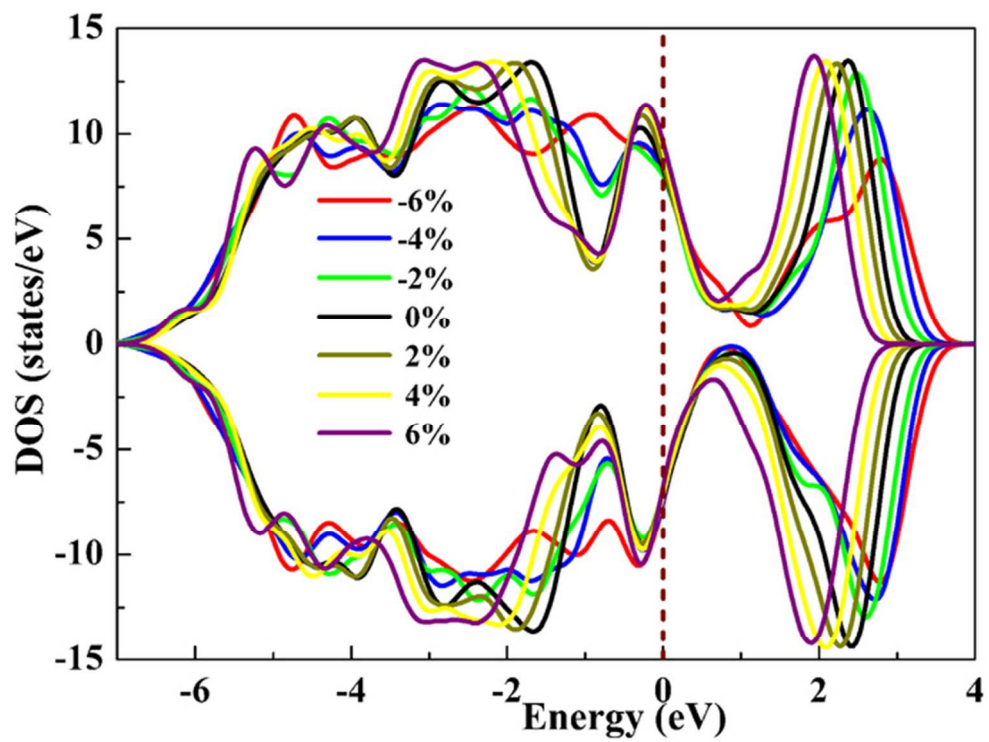38x18mm (300 x 300 DPI)
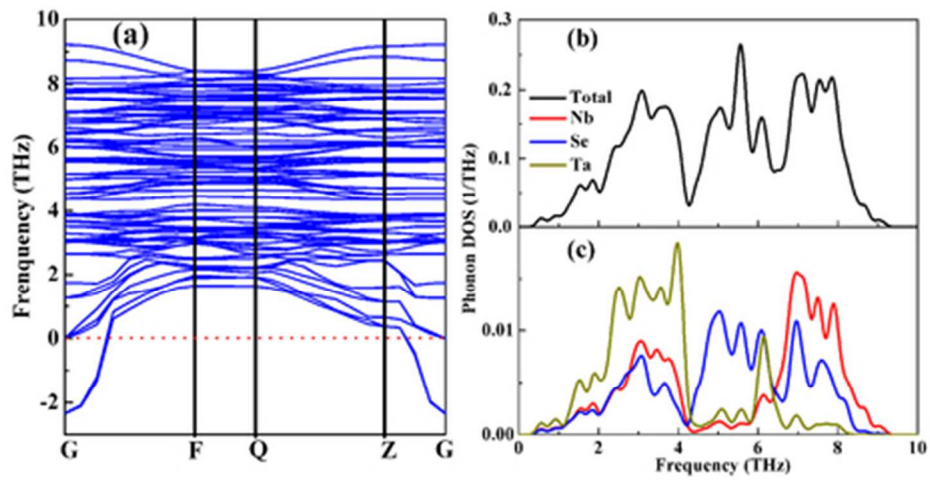
Fig.4
38x18mm (300 x 300 DPI)
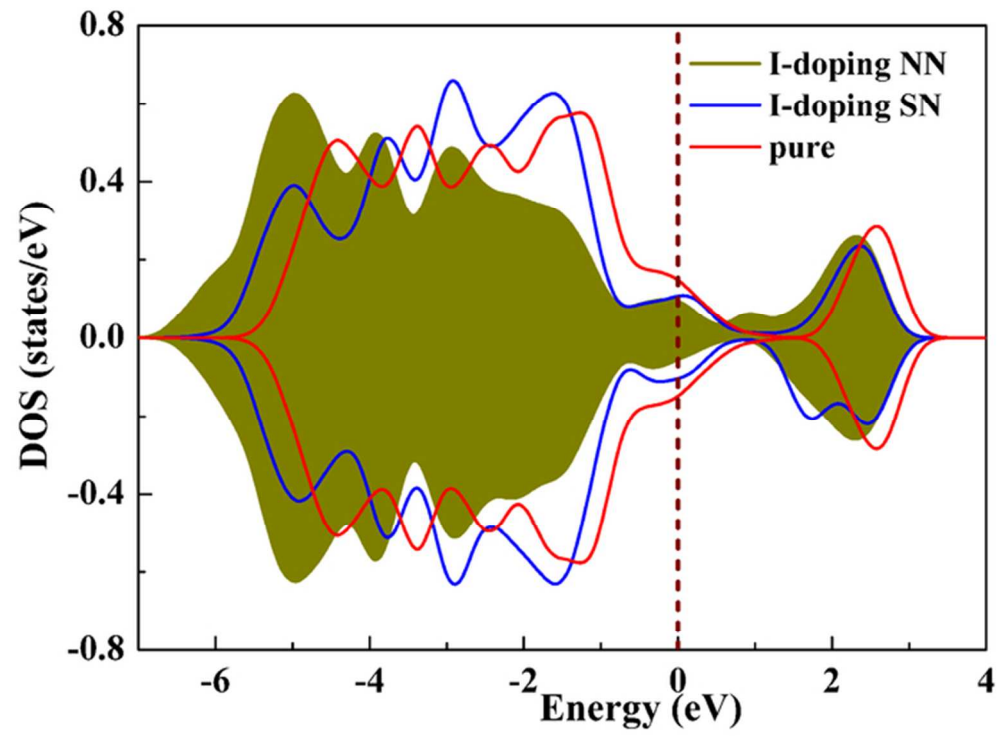
Fig.5
59x43mm (300 x 300 DPI)

Fig.6
59x44mm (300 x 300 DPI)

Fig.7
39x20mm (300 x 300 DPI)